CONF-951007--18

BNL-62646

INVESTIGATION ON THE ELECTROCATALYSIS FOR OXYGEN REDUCTION REACTION BY Pt AND BINARY Pt ALLOYS: AN XRD, XAS AND ELECTROCHEMICAL STUDY

Sanjeev Mukerjee, James McBreen
Department of Applied Science, Brookhaven National Laboratory
Upton, New York 11973

Supramaniam Srinivasan
Center for Electrochemical Systems and Hydrogen Research
Texas Engineering Experiment Station
Texas A&M University, College Station, Texas 77843

ABSTRACT

Electrocatalysis for the oxygen reduction reaction (ORR) on five binary Pt alloy electrocatalysts (PtCr/C, PtMn/C, PtFe/C, PtCo/C and PtNi/C) supported on carbon have been investigated. The electrochemical characteristics for ORR in a proton conducting fuel cell environment has been correlated with the electronic and structural parameters determined under *in situ* conditions using XANES and EXAFS technique respectively. The results indicate that all the alloys possess higher Pt 5*d* band vacancies as compared to Pt/C. There is also evidence of lattice contraction in the alloys (supported by XRD results). Further, the Pt/C shows increase in Pt 5 *d* band vacancies during potential transitions from 0.54 to 0.84 V vs. RHE, which has been rationalized on the basis of OH type adsorption. In contrast to this, the alloys do not exhibit such an enhancement. Detailed EXAFS analysis supports the presence of OH species on Pt/C and its relative absence in the alloys. Correlation of the electrochemical results with bond distances and *d*-band vacancies show a volcano type behavior with the PtCr/C on top of the curve.

INTRODUCTION

The importance of the oxygen reduction reaction (ORR) in low and medium temperature acid fuel cells has been well recognized (1). In an effort towards higher activities for ORR, several Pt alloys were discovered with improved performance first in phosphoric acid (PAFC) (2) and later in proton exchange membrane fuel cells (PEMFC) (3-4). Further, improved long term stability has also been reported for alloy electrocatalysts (3-4). Several investigations have been carried out to determine the role of alloying in the electrocatalytic activity (detailed review in ref., 5), the answer however remains elusive. Based on these previous investigations and in the context of the ORR mechanisms, the principle explanations for the enhanced ORR activity could be enumerated as being due to (i) modification of the electronic structure of Pt (5 *d*-orbital vacancies); (ii) changes in the physical structure of Pt (Pt-Pt bond distance and coordination number); (iii) adsorption of oxygen containing species from the electrolyte on

to the Pt or alloying element; and/or (iv) redox type processes involving the first row transition alloying element (6).

X-ray absorption spectroscopy (XAS) technique with the near edge part (X-ray absorption near structure, XANES) and higher energy side of the spectra (X-ray absorption fine structure, EXAFS) offers the prospect for investigating these factors and their interplay under *in situ* conditions. Details of this technique as applied to electrochemical systems have been reviewed recently (7). This investigation focuses on five binary Pt alloy electrocatalysts (with first row transition metal alloying elements ranging from Cr to Ni) to elucidate the dependence of electrode kinetics for oxygen reduction in terms of their electronic and structural parameters.

EXPERIMENTAL

Five carbon supported binary Pt alloy electrocatalysts (PtCr, PtMn, PtFe, PtCo and PtNi) were procured from Johnson Matthey Inc. (NJ, USA). Based on previous investigations (8-9) the electrocatalyst loading was chosen as 20% (by weight) metal on carbon; the Pt loading in the electrode (for both Pt/C and the Pt alloy electrocatalysts) was 0.3 mg/cm^2 (confirmed by atomic absorption spectroscopy). Details of the electrocatalysts and electrode specifications are given elsewhere (10). XRD measurements on the electrocatalyst powder were carried out using a Sintag automated Diffractometer. Details of these measurements are given elsewhere (10). The electrodes were incorporated into a membrane electrode assembly using the Aciplex® S1004 (Asahi Chemical Co., Japan) proton conducting membrane. Electrochemical characterization was conducted in a cell fixture which allowed both single and half cell measurements using test station which allowed control of the cell temperature, pressure, humidification of the reactant gases, gas flow rate measurements and evaluation of half and single cell potentials as a function of current density. The electrocatalytic activities for ORR were evaluated at 95°C and 5 atm pressure. Similar measurements were also made at several temperatures and pressures for the determination of activation energy and reaction order (in terms of oxygen) for the ORR rate determining step. The temperature variation (35-80°C) were carried out at a nominal constant pressure of 1.33 atm. The pressure variations (1-5 atm.) were similarly carried at a constant temperature of 70°C. Details of the electrochemical cell, test station and the methodologies for preparation of the membrane electrode assembly is given elsewhere (3,11).

The XAS measurements were conducted at the National Synchrotron Light Source (NSLS), Brookhaven National Laboratory using the Beam line X23A2 belonging to the National Institute of Science and Technology (NIST). Measurements were carried out at the Pt L_3 & L_2 and the alloying element K edges. The design of the cell fixture, and electrodes were such that the transmission mode provided adequate step heights. Only in the case of Cr K edge was it necessary to resort to measurement in the fluorescence mode. Details of the spectroelectrochemical cell, data acquisition, monochromator design & resolution and electrode preparation are described elsewhere (10-11). The potential control for in situ XAS was carried out using a potentiostat (Stonehart Associates, Model

BC-1200) and a function generator (Princeton Applied Research, Model 175). The measurements were made at open circuit and at 0.0, 0.24, 0.54 and 0.84 V vs. RHE. The scan rate for potential transitions was 1 mV/s. The K edge XAS measurements for the alloying elements were also made at 1.14 V to check for its stability. Detailed XANES and EXAFS measurements were carried out 0.54 and 0.84 V due to the former being in the double layer region (minimal interference due to oxygen, hydrogen and ionic adsorption) and the latter being in the region where there is adsorption of oxygenated species on the unalloyed Pt surface and lies in the activation controlled region for ORR.

RESULTS AND DISCUSSION

XRD and Electrochemical Characterization

The powder diffraction pattern for the Pt alloy electrocatalysts reveal that all the alloy electrocatalysts form Intermetallic crystalline structures comprising of a primary superlattice phase with Pt_3M (where M is the first row transition element) stoichiometry possessing LI_2 type lattice with fcc structure. This was based on comparisons with the standard JCPDS data base and reference (12-17). The lattice parameters for the Pt alloys, reveal contractions in comparison to that for the Pt/C electrocatalyst (Table 1). The particle size based on the X-ray line broadening of the principle (<111>) diffraction line (full width at half maximum) were estimated using the Scherrer equation (18) (Table 1). As evident from these values, the alloying causes an increase in the particle size.

Table 2 shows the electrode kinetic parameters for oxygen reduction at 95°C and 5 atm. pressure. As evident from the comparison of the exchange current densities, potential at 10mA/cm^2 and current density at 900 mV (activation polarization region), all Pt alloys exhibit enhanced electrocatalytic activities on a per geometric area basis with the highest enhancement shown by PtCr/C. The roughness factors determined from the hydrogen desorption peaks of the cyclic voltammograms show similar values for both Pt and Pt alloys with the alloys showing slightly smaller values (Table 2). The electrocatalytic activities normalized on the basis of these roughness factors therefore follow a similar trend as observed in terms of the geometric area (Table 2). Among the other Tafel parameters, the Tafel slope remained invariant, ranging between 62 to 65 mV/decade for both Pt and Pt alloy electrocatalysts.

The Tafel kinetic parameters were similarly obtained for three selected Pt alloys (PtCr/C, PtCo/C and PtNi/C) as a function of temperature (35-80°C). The activation energies for ORR, obtained from the slopes of the Arrhenius type plots (Log i_{900mv} vs. 1/T), show lower values for the Pt alloys as compared to Pt/C (Table 2). This result is consistent with the higher electrocatalytic activities for ORR exhibited by these alloys and followed the same trend with PtCr/C having the lowest activation energy. These different activation energies for the alloys as compared to Pt/C is indicative of changes in the electronic and structural characteristics of Pt. Since this could be indicative of a different rate determining step (as enumerated in Figure 1) an evaluation of the Tafel kinetic parameters was conducted as a function of oxygen pressure (1-5 atm.). This allowed the

determination of reaction orders for ORR with respect to dioxygen. These were obtained from the slopes of log i_o vs log P_o plots (Table 2). The reaction orders obtained indicate no difference for Pt and Pt alloys. This suggests the possibilities of reaction pathways I or II for Pt and Pt alloys (Figure 1).

In situ XANES and EXAFS Characterization

One of the significant aspects of XANES analysis is that it can provide important information on the Pt 5 *d*-band vacancies. The 5 *d*-band vacancies were derived from integration of peak intensities of the Pt L_3 and L_2 XANES spectra. Since these spectra are based on transitions from $2p_{3/2}$ and $2p_{1/2}$ to $5d_{5/2}$ orbital, they reflect vacancies in the latter orbitals based on direct proportion to the spectrum intensities. The theoretical and methodological aspects of this determination is provided elsewhere (10-11). Figure 2 (a) shows the Pt L_3 XANES spectrum for Pt/C at 0.54 and 0.84 V vs. a Pt foil. As evident from the spectra, the XANES at 0.54 V shows exact congruence to that of the pure Pt foil in contrast to the increase in intensity exhibited at 0.84 V. This figure not only confirms the lack of ionic and other interferences at 0.54 V but also indicates an increase in *d*-band vacancies at 0.84 V. Similar comparison for the alloys, shown by the representative spectra for PtCo/C in figure 2 (b) indicates that (*i*) the alloys have higher 5 *d*-band vacancies (when compared at 0.54 V) and (*ii*) there is negligible change in spectral intensity and hence *d*-band vacancy during potential transition to 0.84 V. These observations are quantitatively represented in terms of values for the *d*-band vacancies in Table 3. The possible exception to these results is the PtMn/C, which can be interpreted to be a result of the stable $3s^24d^5$ electronic configuration of Mn. The other elements exhibit increase in the *d*-band vacancies based on the electronic affinities of the alloying element.

The EXAFS analysis involved Fourier filtering of the isolated EXAFS spectra (Pt L_3 edge) using *k*-space windows (Δk range) as described in Table 4. The corresponding Fourier transform allowed isolation of a limited number of shells using inverse Fourier transform (Δr ranges in Table 4) for analysis using iterative least square fitting with the experimentally and theoretically derived phase and amplitude parameters of standards. The approach taken for fitting the data was to chose the simplest model first and attempt to fit the data. The standard reference materials used in this work was the liquid N_2 data for a pure Pt foil (5μm thick) and the octahedrally coordinated complex $Na_2Pt(OH)_6$ for the Pt-Pt and Pt-O, phase and amplitude parameters respectively. For the Pt-M phase and amplitude parameters theoretical calculations based on the FEFF programs were used with Cartesian coordinates from a fcc lattice structure. The limits of error in the EXAFS analysis and the methodologies adopted are given elsewhere (10).

Figure 3 (a) shows the comparison of the Fourier transforms of the EXAFS for Pt/C at 0.54 and 0.84 V. The Fourier transform at 0.84 V shows peaks related to the presence of oxygenated species at low R values (<2 Å) and a consequent decrease in the Pt-Pt interactions as compared to the corresponding spectra at 0.54 V. Adsorption of oxygenated species could therefore account for the increase in the *d*-band vacancies for Pt/C at 0.84V. A similar comparison for the alloys as shown by the representative figure 3

(b) for the PtCr/C alloy exhibits no change as a result of potential transition from 0.54 to 0.84 V. This fact is further illustrated in Figure 4 (a) which shows a single shell Pt-Pt fit for the Pt/C sample at 0.84V. This figure shows deviation from the fit at low R values due to the presence of chemisorbed oxygen on the Pt surface. In contrast a two shell fit using the Pt-Pt and Pt-O standards gives an excellent fit (figure 4 (b)), thus confirming the earlier hypothesis. These results on the Pt/C electrocatalysts are in agreement with previous XAS investigations on Pt/C electrocatalyst (19-20). Further, theoretical and experimental investigations on the ORR mechanism have shown increased coverage by OH or O species at potentials above 0.8 V and the effect of a Temkin type adsorption isotherm on the electrode kinetic parameters (21). The contrasting result in the alloys (with the possible exception of PtMn/C) appears to be due to electronic properties remaining unchanged at 0.54 and 0.84 V. This is confirmed by the fact that at 0.84 V the Pt alloys could still be fit to a simple two shell Pt-Pt and Pt-M fit, without the need to include a Pt-O contribution. Figure 5 (a) and (b) show this fit in both *k* and *r*-space for a PtCr/C sample at 0.84 V. The results of these EXAFS analysis thereby shows (Table 5) that a change in potential does not effect the bond distances in both Pt and Pt alloys. The coordination numbers show the expected changes for Pt/C due to the chemisorption of oxygenated species beyond 0.8 V and the absence of such effects in the case of Pt alloys. In addition, the smaller coordination numbers obtained for the Pt and Pt alloys reflect the particle sizes of the crystallites in the supported catalyst.

Correlation of the electrochemical kinetic data (i_o, i_{900mV} etc.) with Pt 5 *d*-band vacancies and Pt-Pt bond distances are shown in Figure 6. A volcano type behavior is observed in terms of both the electronic and geometric parameters. The theoretical basis of volcano type behavior (22) indicates that at a fixed P_{O2} and $\{H^+\}$ the rate (log *i*) should illustrate ascending and descending linear functions of ΔG_{OH} with the maximum being at $\Delta G_{OH} = 0$. This approach therefore implies that the Pt/C and PtMn/C electrocatalysts have high overpotentials with $\Delta G_{OH} < 0$, followed by PtCr/C with $\Delta G_{OH} \sim 0$ and PtFe/C , PtCo/C and PtNi/C electrocatalysts again having high overpotentials with $\Delta G_{OH} > 0$. From the results shown above, there are principally three interrelated factors controlling the electrocatalysis of oxygen reduction reaction. These are (a) the vacancies of the Pt 5 *d* orbitals, (b) the Pt-Pt bond distance, and (c) the adsorption characteristics of the oxygenated species from the electrolyte solution. The interplay of a redox type processes was, however, ruled out on the basis of the fact that position of the K-edge XANES of alloying elements were unaffected as a result of potential transition from 0.54 to 1.14 V. A change in the oxidation state, expected as a result of a redox type process is therefore absent. This is illustrated in the case of the PtNi/C alloy electrocatalyst, where there is no change in the Ni K-edge XANES in the potential region of 0.0 V to 1.14 V vs. RHE (Fig. 7). The lack of change in the white line intensities also indicates that there is no corrosion of Ni at positive potentials. Similar results were also found for the other alloys. This result strongly suggests to the possibility of the outer surface of the alloy to be mostly comprised of Pt.

CONCLUSIONS

(A) All the alloys possess higher Pt *d* band vacancies as compared to Pt/C.

(B) *In situ* EXAFS analysis indicates contraction of Pt-Pt bond distances for all the alloys as compared to Pt/C.

(C) The bond distances and the Pt 5 *d* band character indicates a smooth and inverse relationship. Comparison of $(h_J)_{t_{2g}}$ at 0.54 and 0.84 V indicates an increase for Pt/C in contrast to the alloy electrocatalysts. This can be rationalized on the basis of OH type adsorption onto the Pt surface in Pt/C and its relative absence in the alloys. This is further confirmed by EXAFS analysis at the Pt L_3 edge. The bond distances for both Pt and Pt alloys remain unaffected as a result of this potential transition. The Pt/C however does show change in the coordination numbers due to adsorption of oxygenated species beyond 0.8 V in contrast to the Pt alloys.

(D) Correlation of XAS results with the electrocatalytic activities exhibit Volcano type behavior.

(E) XANES analysis at the alloying element K edge indicates absence of any redox type mechanism. These results indicate the possibility of different extents of surface enrichments of Pt in the supported alloy electrocatalysts.

ACKNOWLEDGMENTS

The authors gratefully acknowledge the support of the National Aeronautic and Space Administration-Johnson Space Center under the auspices of the Regional University Grant Program (Grant # NAG 9-533), Center for Energy and Mineral Resources, Texas A&M University and the U.S. Department of Energy, Division of Material Science, Brookhaven National Laboratory (Contract # DEA-CO2-76CH00016) for its role in the development and operation of the National Synchrotron light Source (NSLS). The help of NIST personnel at the Beam Line X23A2 in particular Joe Woicik and John Kirkland is gratefully acknowledged. The authors gratefully acknowledge Lindsay Keck of Johnson Matthey Inc., who supplied the electrocatalysts. The experimental work at Brookhaven was supported by the Office of Transportation Technologies, Electric and Hybrid Vehicles Division of U.S. Department of Energy.

REFERENCES

(1) A. J. Appleby, *Energy*, **11**, 13 (1986).
(2) D. A. Landsman and F. J. Luczak, *U. S. Patent*, 4,316,944 (1982).
(3) S. Mukerjee and S. Srinivasan, *J. Electroanal. Chem.*, **357**, 201 (1993).
(4) G. Tamizhmani and G. A. Capuano, *J. Electrochem. Soc.*, **141**, 968 (1994).
(5) S. Mukerjee, *J. Appl. Electrochem.*, **20**, 537 (1990).
(6) R. Parsons and T. Vandernoot, *J. Electroanal. Chem.*, **257**, 9 (1988)
(7) H. D. Abruna, *Electrochemical Interface: Modern Techniques for In situ Interface Characterization*, VCH Publishers Inc., New York (1991).

(8) E. A. Ticianelli, C. R. Derouin and S. Srinivasan, *J. Electroanal. Chem.*, **251**, 275 (1988).
(9) S. Srinivasan, E. A. Ticianelli, C. R. Derouin and A. Redondo, *J. Power Sources*, **22**, 359 (1988).
(10) S. Mukerjee, S. Srinivasan, M. P. Soriaga and J. McBreen, *J. Phys. Chem.*, **99**, 4577 (1995).
(11) S. Mukerjee, S. Srinivasan, M. P. S. Soriaga and J. McBreen, *J. Electrochem. Soc.*, **142**, 1409 (1995).
(12) T. Swanson, *Natl. Bur. Stand. (U.S), Circ.*, **1,31**, 539 (1953).
(13) J. Baglin, *J. Electrochem. Soc.*, **125**, 1854 (1978).
(14) E. Raub and W. Mahler, *Z. Mettalk.*, **46**, 210 (1955).
(15) A. Kussman and G. G. V. Rittberg, *Z. Mettalk.*, **41**, 470 (1950).
(16) A. H. Geisler and D. L Martin, *J. Appl. Phys.*, **23**, 375 (1952).
(17) C. Leroux, C. Cadeville, V. Pierron-Bohnes, G. Inden and F. Hinz, *Phys. F: Met. Phys.*, **18**, 2033 (1988).
(18) H. Klug and L. Alexander, *X-ray Diffarction Procedures*, Wiley, NewYork, (1962) p491.
(19) M. E. Herron, S. E. Doyle, S. Pizzini, K. J. Roberts, J. Robinson, G. Hards and F. C. Walsh, *J. Electroanal. Chem.*, **324**, 243 (1992).
(20) P. G. Allen, S. D. Conradson, M. S. Wilson, S. Gottesfeld, I. D. Raistrick, J. Valerio and M. Lovato, *Electrochim. Acta.*, **39**, 2415 (1994).
(21) M. R. Tarasevich, *Electrokhimya*, **9**, 59 (1973).
(22) A. J. Appleby, *Catal Rev.*, **4**, 221 (1970).

Table 1

Structural characteristics of Pt and Pt alloy electrocatalysts, as obtained from XRD studies

Electrocatalyst	Pt/C	PtMn/C	PtCr/C	PtFe/C	PtCo/C	PtNi/C
Lattice Parameter Pt-Pt Bond distance (Å)	3.927 (2.777)	3.898 (2.756)	3.873 (2.738)	3.866 (2.733)	3.854 (2.725)	3.812 (2.695)
Average Particle Size (Å)	35	69	57	58	69	58

Table 2

Electrode kinetic parameters for oxygen reduction on Pt and Pt alloy electrocatalysts in proton exchange membrane fuel cells at 95°C and 5 atm pressure. Pt loading in electrodes 0.3 mg/cm^2.

Electrocatalyst	i_o mA/cm^2 (10^4)	i_{900mV} mA/cm^2	E_{10mA/cm^2} mV	Roughness Factor cm^2/cm^2	i_o* mA/cm^2 (10^5)	$\Delta H_{activation}$ KJ/Mole	nO_2 log i_o/ logP_o
Pt/C	3.46	22.1	915	61	0.56	62.17	0.96
PtMn/C	6.26	40.1	945	48	1.30	-	-
PtCr/C	7.15	83.8	951	50	1.43	27.63	0.97
PtFe/C	6.94	50.4	948	56	1.36	-	-
PtCo/C	5.87	37.2	935	49	1.19	35.44	0.85
PtNi/C	4.86	26.4	924	48	1.01	43.23	0.89

* Normalized with respect to the electrochemically active surface area

Table 3

Calculated 5 *d*-band vacancies for Pt and Pt alloy electrocatalysts as obtained from *in situ* XANES spectra (Pt L_3 and L_2 edges) at 0.54 and 0.84 V vs RHE.

Electrocatalyst	Pt/C	PtMn/C	PtCr/C	PtFe/C	PtCo/C	PtNi/C
$(h_j)_{t,s}$ at 0.54 V	0.329	0.331	0.360	0.368	0.401	0.409
$(h_j)_{t,s}$ at 0.84 V	0.370	0.344	0.358	0.370	0.398	0.404

Table 4

Fourier transformation ranges of the forward and inverse transforms (k^3 weighted) for Pt/C and Pt alloy electrocatalysts at the double layer and oxygen reduction regions

	(0.54 V vs. RHE)		(0.84 V vs. RHE)	
Electrocatalyst	Δk (Å^{-1})	Δr (Å)	Δk (Å^{-1})	Δr (Å)
Pt/C	3.49-14.23	1.40-3.05	3.26-14.15	1.3-3.04
PtCr/C	3.15-14.71	1.41-3.41	3.15-14.71	1.50-3.41
PtMn/C	3.70-14.22	1.21-3.61	2.73-17.42	1.04-3.52
PtFe/C	3.45-17.14	1.50-3.40	3.68-17.45	1.50-3.40
PtCo/C	3.22-14.61	1.50-3.50	3.22-14.76	1.50-3.40
PtNi/C	3.55-14.64	1.50-3.50	3.55-14.85	1.30-3.50

Table 5

Results of *in situ* EXAFS analysis at the Pt L_3 edge for Pt/C electrocatalyst at 0.54 and 0.84 V vs. RHE.

Coordination Shell	EXAFS Parameter at 0.54 V vs. RHE		EXAFS Parameter at 0.84 V vs. RHE	
	N	R (Å)	N	R (Å)
Pt-Pt	8.66	2.773	6.73	2.773
Pt-O			1.69	2.037

Errors were typically 1 to 8% (N) & 0.005 to 0.01 Å (R) for single shell fits

Results of *in situ* EXAFS analysis at the Pt L_3 edge for supported Pt alloy electrocatalysts at 0.54 V vs. RHE.

Coordination Shell	EXAFS Parameter	Alloying Element				
		Mn	Cr	Fe	Co	Ni
Pt-Pt	N	7.52	8.53	6.71	6.94	9.12
	R	2.762	2.713	2.701	2.684	2.683
Pt-M	N	2.75	2.78	2.98	2.48	2.72
	R	2.682	2.690	2.640	2.631	2.613

Errors were typically 5 to 14% (N) & 0.007 to 0.012 Å (R) for two shell fits

Results of *in situ* EXAFS analysis at the Pt L_3 edge for supported Pt alloy electrocatalysts at 0.84 V vs. RHE.

Coordination Shell	EXAFS Parameter	Alloying Element				
		Mn	Cr	Fe	Co	Ni
Pt-Pt	N	8.31	8.82	6.40	7.62	9.45
	R	2.762	2.713	2.711	2.684	2.683
Pt-M	N	2.86	2.89	2.43	2.34	3.34
	R	2.681	2.700	2.652	2.631	2.583

Errors were typically 5 to 14% (N) & 0.007 to 0.012 Å (R) for two shell fits

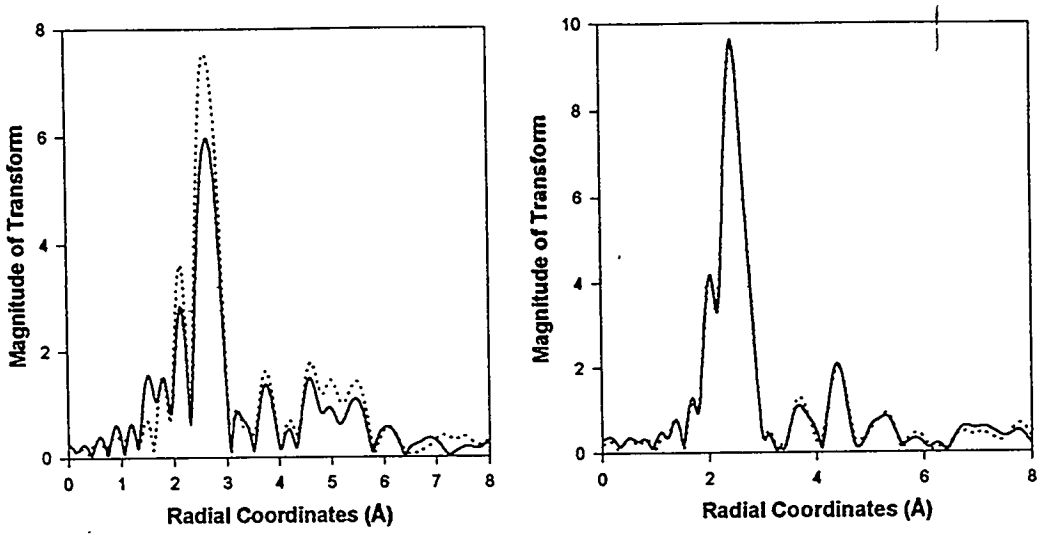

(a) (b)

Figure 3. Comparison of Fourier transform (k^3 weighted) at 0.54 V (...) and 0.84 V (—) vs. RHE for (a) Pt/C and (b) PtCo/C alloy electrocatalyst. (Δk values in Table 4).

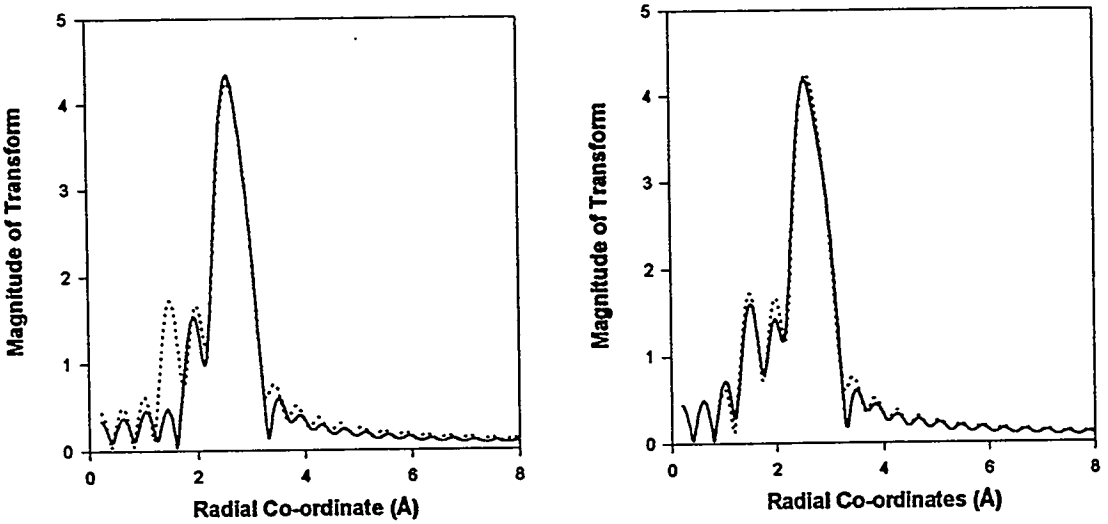

(a) (b)

Figure 4. Fits to the data (...) for a Pt/C catalyst at 0.84 V in r space; (a) a single Pt-Pt shell fit (—), (b) a two shell, Pt-Pt and Pt-O, fit (—). k^3 weighted, Δk values in Table 4.

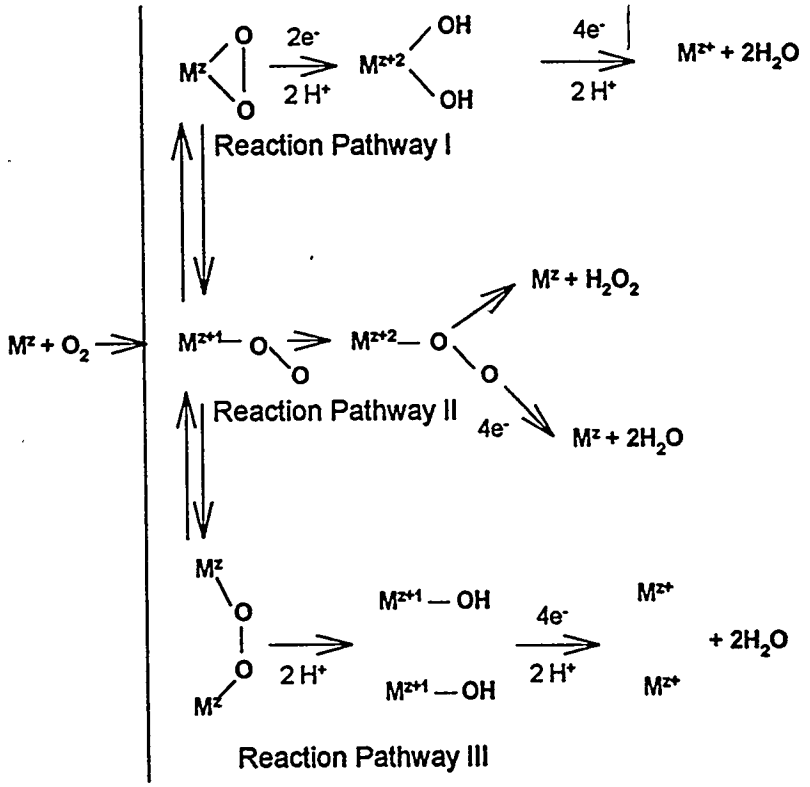

Figure 1. Reaction pathways for oxygen electro-reduction in acid electrolytes.

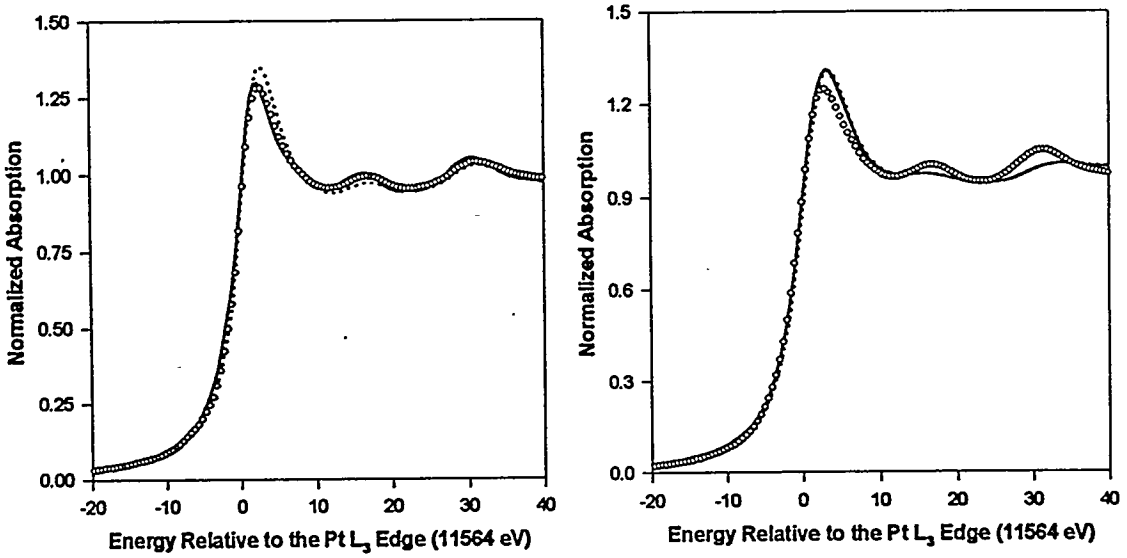

Figure 2. XANES at the Pt L_3 edge for (a) Pt/C and (b) PtCo/C at 0.54 (—) and 0.84 V (...) vs a pure Pt foil reference standard (O).

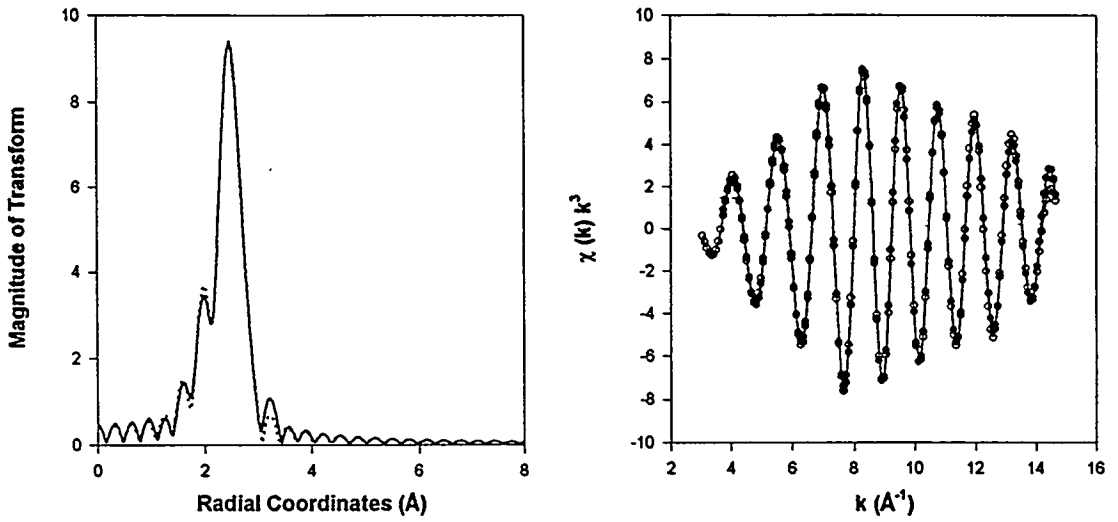

(a) (b)

Figure 5. A two shell fit (Pt-Pt and Pt-Cr) for the EXAFS of PtCr/C sample at 0.84 V in (a) *r*-space and (b) *k*-space. The fits are k^3 weighted with the sample data denoted by [(...) in *r* and (O) in *k* space] and the fitted data by [(—) in *r* and (●) in *k* space].

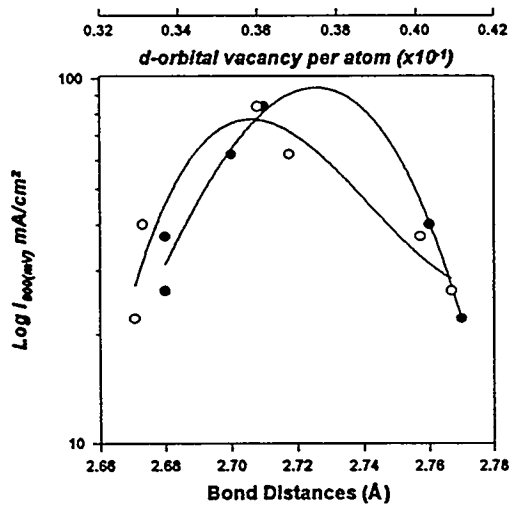

Figure 6. Correlation of oxygen electrode performance of Pt and Pt alloy electrocatalysts in proton exchange membrane fuel cell with Pt-Pt bond distance (●) and *d*-orbital vacancy of Pt (O).

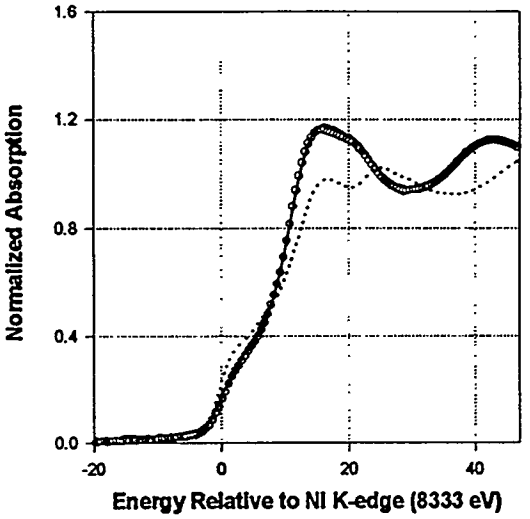

Figure 7. XANES at the Ni K edge for PtNi/C electrocatalyst at 0.54 (—) and 1.14 V (O) relative to the pure Ni foil reference standard (...).